

## Design, simulation, and static testing of an eco-friendly prosthetic foot using ramie-PLA composite

Iyan Sopiyan<sup>1</sup>, Tresna P. Soemardi<sup>\*</sup>, Herry Purnomo<sup>2</sup>, and Olivier Polit<sup>3</sup>

<sup>1</sup> Department of Mechanical Engineering, Faculty of Engineering, Universitas Indonesia, **Indonesia**

<sup>2</sup> Aeronautics and Spaces Research Organization, Badan Riset dan Inovasi Nasional (BRIN), **Indonesia**

<sup>3</sup> Laboratoire Energétique Mécanique Electromagnétisme, Université Paris Nanterre, **France**

\* Corresponding Author: [tsoemardi@eng.ui.ac.id](mailto:tsoemardi@eng.ui.ac.id)

*Received:* 05 April 2025; *Revised:* 05 June 2025; *Accepted:* 07 June 2025

 Cite this <https://doi.org/10.24036/teknomekanik.v8i1.36572>

**Abstract:** This study developed a sustainable lower-limb prosthetic prototype using biodegradable ramie fiber-reinforced PLA composite as its primary material. The design specifically addresses the needs of individuals with limb amputation while prioritizing environmental sustainability. PLA-based composites for structural biomedical applications—particularly those in lower-limb prosthetics—must meet rigorous mechanical and fatigue performance requirements under repetitive loading. This study investigates the development of a transtibial prosthetic foot prototype using a quasi-isotropic lay-up prepreg ramie-PLA composite fabricated via the hot press method. Material characterization was conducted per ASTM standards, and the design was evaluated using the Finite Element Method (FEM). The prototype underwent static testing according to ISO 22675 with a user load criterion. The laminate exhibited an ultimate tensile strength of  $48.36 \pm 0.95$  MPa, an elastic modulus of  $4.125 \pm 0.25$  GPa, and a flexural strength of  $62.06 \pm 3.43$  MPa. FEM results showed that all normal and shear stresses during heel strike (17.78 MPa and 1.71 MPa) and toe-off (12.38 MPa and 5.69 MPa) phases remained below fatigue limits. Experimental static stresses were heel strike (12.72 MPa) and toe-off (20.09 MPa), both within safe operational limits. These findings highlight the structural viability and environmental sustainability of ramie-PLA composites, positioning them as a promising material for next-generation prosthetic foot development.

**Keywords:** ramie fibers; PLA; bio-composite; lower limb prosthetic foot; prosthetic design and development

### 1. Introduction

Recent advancements in materials science have significantly influenced the biomedical sector, particularly in the development of intelligent, durable materials for prosthetic limbs and other medical devices [1], [2]. These materials are expected to provide high mechanical strength and thermal stability, along with antibacterial properties in certain applications [3], [4], [5] with biodegradability, renewability, and reduced environmental impact [6], [7]. Rising demand for sustainable technologies has intensified research on natural fiber-reinforced polymers (NFRPs) and green composites. Fiber-reinforced polymer composites are a compelling alternative to traditional metals and ceramics in biomedical and aerospace applications due to their lightweight nature, high stiffness-to-weight ratio, and cost-effectiveness [6]. Among these, ramie fiber-reinforced polylactic acid (PLA) composites have gained attention [7], [8], [9]. In Indonesia, the advancement of natural fiber composites—especially those utilizing locally sourced fibers—has shown significant promise due to their high strength, corrosion resistance, and eco-friendly decomposition [10], [11], [12], [13].

PLA is distinguished by its mechanical properties, particularly tensile strengths frequently exceeding 70 MPa, surpassing common biodegradable polymers like polyhydroxyalkanoates (PHAs) [14], [15]. PLA composites reinforced with ramie fibers improve composite stiffness and tensile performance, but degrade under humid or soil-burial conditions. It requires surface treatments or compatibilizers to increase interfacial adhesion [15], [16]. Prepreg-based fabrication techniques are increasingly preferred for high-performance fiber composites due to process consistency and reliability [17]. Simultaneously, lower-limb prosthetic design has advanced from basic mechanical structures to bionic systems, driven by innovations in material science, biomechanics, and computational modelling [18], [19], [20], [21].

Advanced material technologies have been widely developed in the healthcare business to create smart and innovative materials for prosthetic limb systems with excellent mechanical qualities and extended durability. However, research and development of environmentally friendly prosthetic limbs remain limited. Green materials innovations align with Sustainable Development Goal 9 (Industry, Innovation, and Infrastructure) while improving quality of life. These composites provide significant weight reduction, enhanced performance, and design adaptability [22], [23], [24]. Current prosthetic foot commonly utilize carbon fiber composites, which exhibit exceptional strength and rigidity [4], [25], [26] but the non-biodegradable and non-renewable nature of carbon fiber presents significant environmental challenges [27], [28]. Therefore, the biocompatibility and mechanical properties of ramie-PLA composites represent a promising material choice for biomedical applications, particularly in prosthetic foot development.

Lower-limb amputations encounter significant mobility limitations for approximately 37 million people worldwide. These individuals often experience diminished quality of life through physical barriers, social stigmas, and increased injury risk [29]. Transtibial amputees require 10–40% more energy expenditure to maintain normal walking speed and elevated oxygen consumption compared to non-amputees [30], [31], [32], [33]. These limitations often restrict participation in daily activities. Additionally, prosthetic services remain frequently inaccessible or cost-prohibitive, particularly for individuals in lower socioeconomic communities [34], [35]. To address these limitations, this study aims to design and develop a cost-effective, sustainable transtibial prosthetic foot prototype using ramie-PLA bio-composite laminates. It focuses on structural design, fabrication via hot press prepreg methods, and mechanical performance validation using finite element analysis and standardized static testing (ASTM and ISO 22675).

## 2. Material and methods

The methodology employed in this study consists of three main stages: material and testing validation, design and analysis, and prototype fabrication, followed by mechanical properties testing. Initially, ramie-PLA composite laminates were manufactured using a hot press prepreg method. The experimentally characterized mechanical properties were implemented as material inputs for ANSYS Workbench finite element simulations. Based on the simulation results, a prosthetic foot prototype was fabricated and subsequently subjected to static testing to evaluate its performance.

### 2.1 Material and testing validation

Ramie fibers were supplied by Nantong Yemeng New Material Co., Ltd., and the PLA matrix (Biopoly 103 granules) was procured from Shanghai Huiang Industrial Co., Ltd. To enhance fiber-matrix adhesion, isophorone diisocyanate (IPDI) was used as a compatibilizer, in combination with 0.5% Tin (II) octoate (Santa Cruz Biotechnology) and 0.5% triphenyl phosphite (TPP) (Tokyo Chemical Industry Co., Ltd.). Dichloromethane (DCM), used as the solvent, was supplied by PT. Indogen Intertama.

Based on a previous study, a formulation of 1.5% IPDI, 0.5% Tin (II) octoate, and 0.5% TPP by total weight of the composite was adopted to achieve optimal mechanical performance [16]. The PLA granules were dissolved in DCM at a 1:6 (w/v) ratio under magnetic stirring for 2 hours. The compatibilizers were subsequently added and mixed for 10 minutes at room temperature. The ramie fibers were manually woven with unidirectional orientation and a cotton binder in the horizontal direction. The woven fabric was then impregnated with the PLA/DCM solution until fully saturated. The resulting prepreg was removed, wrapped in parchment paper, and stored at  $-18^{\circ}\text{C}$  for 14 days before further processing.

Laminate specimens were manufactured using an aluminum mold ( $254 \times 194 \text{ mm}^2$ , AA 6061-T6) under hot-press conditions ( $110^{\circ}\text{C}$ , 132 bar, 90 minutes). The cured sheets were then laser-cut into test specimens for mechanical characterization. The volume fraction was controlled at approximately 45% fiber ( $V_f$ ) and 55% matrix ( $V_m$ ). These experimentally determined material properties served as input parameters for subsequent finite element analysis in ANSYS. The properties of the laminate composite ramie-PLA were performed in previously researched by the authors, summarized in Table 1. These lamina properties were subsequently input into ANSYS for Finite Element Analysis of the prosthetic foot geometry.

**Table 1.** Lamina Material Properties [36]

Properties	Value	Unit
$(\sigma_1^T)_{ult}$	80.07	[MPa]
$(\sigma_2^T)_{ult}$	33.38	[MPa]
$(\tau_{12})_{ult}$	31.79	[MPa]
$(\sigma_1^C)_{ult}$	31.77	[MPa]
$(\sigma_2^C)_{ult}$	38.09	[MPa]
$E_1$	10.38	[GPa]
$E_2$	1.6	[GPa]
$G_{12}$	2.04	[GPa]
$\nu_{12}$	0.28	-

The lamina properties obtained will be used to determine the stack-up laminate isotropic orientation layup configuration and mechanical analysis for the prosthetic foot design, using established basic composite laminate mechanics equations. For validation of its mechanical properties, the ramie-PLA prosthetic foot will undergo ASTM standard tests at ambient temperature for tensile and flexural. Mechanical testing includes: tensile testing of laminate composite ramie-PLA per ASTM D3039 (speed of 3 mm/min), flexural testing per ASTM D7264 (speed of 1 mm/min), and tensile testing for EVA (Ethylene-Vinyl Acetate) per ASTM D3574 (speed of 500 mm/min) to ensure that the prosthetic foot meet the required mechanical properties [34-38]. Mechanical testings were conducted using equipment available at the Badan Riset dan Inovasi Nasional (BRIN) laboratory in Indonesia.

Tensilon UTM RTG-1250 machine was employed to obtain tensile properties and flexural test with 10 kN load cell, and 1 kN load cell for the EVA tensile test. A general-purpose Kyowa KFGS-5-120-D16-11 L3M2S strain gauge is designed to measure strain and data acquisition rate of 200 Hz. Following the analysis, a Scanning Electron Microscope (SEM) was utilised to investigate the failure of the specimens.

$$\begin{bmatrix} \sigma_x \\ \sigma_y \\ \tau_{xy} \end{bmatrix} = \begin{bmatrix} \cos^2 \theta & \sin^2 \theta & -2\sin\theta\cos\theta \\ \sin^2 \theta & \cos^2 \theta & 2\sin\theta\cos\theta \\ \sin\theta\cos\theta & -\sin\theta\cos\theta & \cos^2 \theta - \sin^2 \theta \end{bmatrix} \begin{bmatrix} \sigma_1 \\ \sigma_2 \\ \tau_{12} \end{bmatrix} \quad (1)$$

## 2.2 Design and analysis

The design of the prosthetic foot was based on a combination of standard biomechanical modeling and finite element simulation to ensure structural integrity under dynamic loading conditions. A prosthetic structure capable of absorbing impact and providing suspension effects was the target of the study. Finite element simulations were conducted using ANSYS Workbench, per ISO 22675 standards and modifications derived from the AOPA's prosthetic foot protocol to account for variable user loads [37], [38], [39]. A user body mass of 65 kg was assumed in the simulation, corresponding with gait analysis data that define loading conditions during heel strike and toe-off phases. A walking speed of 1.43 m/s generates a peak ground reaction force equivalent to 120% of body weight (BW) at heel strike and approximately 110% of BW at toe-off [37], [38].

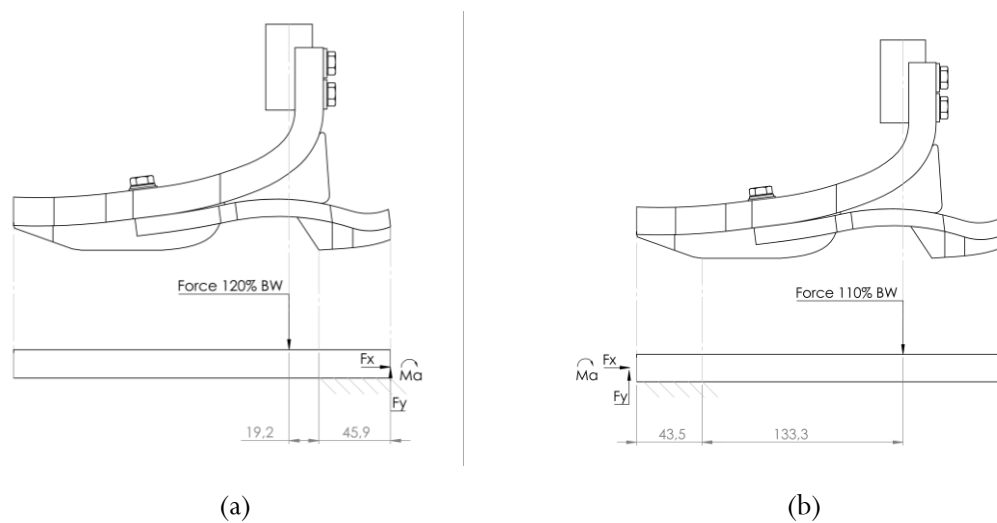


**Figure 1.** Heel strike and Toe-off phases

The preliminary dimensions of the prosthetic foot are determined via mathematical modelling, incorporating dynamic load parameters to ensure functionality under anticipated dynamic stress. Initial design calculations for minimum thickness were based on laminate beam theory and dynamic tensile stress limits of ramie-PLA composites [40].

$$\sigma_{dn} = \frac{M \cdot y}{I} \quad (2)$$

$$I = \frac{B \cdot h^3}{12} \quad (3)$$

$$y = \frac{h}{2} \quad (4)$$

$$h_{min} = \sqrt{\frac{M \cdot .6}{B \cdot \sigma}} \quad (5)$$

From the given equation, the maximum moment (M) is determined from the model's width (B), its thickness (h), and the dynamic tensile strength ( $\sigma_{dn}$ ) of quasi-isotropic ramie-PLA composite at  $10^6$  cycles. The minimum thickness, derived from the previous requirements, is subsequently simulated to verify that peak stresses remain below the allowable limit. Composite simulations in

finite element analysis were performed in ANSYS ACP software (licensed via BRIN), incorporating material properties from the previously characterized ramie-PLA lamina. The angles formed from each phase are 15° in Hell Strike and 20° in toe-off [38], [39], [41]. The analysis identified peak stress regions on the prosthetic structure, and the design was iteratively refined to maintain a dynamic safety factor no lower than 1. Dynamic safety factors were determined from extracted stress value from the ANSYS model simulations and plotted using the Tsai-Wu and Norris-McKinnon failure criteria. The Tsai-Wu criterion for composite is defined as follows:

$$H_1\sigma_1 + H_2\sigma_2 + H_6\tau_{12} + H_{11}\sigma_1^2 + H_{22}\sigma_2^2 + H_{66}\tau_{12}^2 + 2H_{12}\sigma_1\sigma_2 = 1 \quad (6)$$

The five strength parameters for a unidirectional laminate were used to derive the following formula and its components,  $H_1$ ,  $H_2$ ,  $H_6$ ,  $H_{11}$ ,  $H_{22}$ , and  $H_{66}$ . Where,  $\sigma_1 = (\sigma_x^T)_{ult}$  ultimate tension stress x direction,  $\sigma_2 = (\sigma_y^T)_{ult}$  ultimate tension stress y direction,  $\tau_{12} = (\tau_{xy})_{ult}$  Ultimate shear stress on xy plane and  $\sigma_1 = -(\sigma_x^C)_{ult}$  is ultimate compression stress on x direction, and  $\sigma_2 = (\sigma_y^C)_{ult}$ , is ultimate compression stress on y direction.

$$H_1(\sigma_1^T)_{ult} + H_{11}(\sigma_1^T)_{ult}^2 = 1 \quad (7)$$

$$-H_1(\sigma_1^C)_{ult} + H_{11}(\sigma_1^C)_{ult}^2 = 1 \quad (8)$$

$$H_1 = \frac{1}{(\sigma_1^T)_{ult}} - \frac{1}{(\sigma_1^C)_{ult}} \quad (9)$$

$$H_{11} = \frac{1}{(\sigma_1^T)_{ult}(\sigma_1^C)_{ult}} \quad (10)$$

$$H_2(\sigma_2^T)_{ult} + H_{22}(\sigma_2^T)_{ult}^2 = 1 \quad (11)$$

$$-H_2(\sigma_2^C)_{ult} + H_{22}(\sigma_2^C)_{ult}^2 = 1 \quad (12)$$

$$H_2 = \frac{1}{(\sigma_2^T)_{ult}} - \frac{1}{(\sigma_2^C)_{ult}} \quad (13)$$

$$H_{22} = \frac{1}{(\sigma_2^T)_{ult}(\sigma_2^C)_{ult}} \quad (14)$$

$$H_6(\tau_{12})_{ult} + H_{66}(\tau_{12})_{ult}^2 = 1 \quad (15)$$

$$-H_6(\tau_{12})_{ult} + H_{66}(\tau_{12})_{ult}^2 = 1 \quad (16)$$

$$H_6 = 0 \quad (17)$$

$$H_{66} = \frac{1}{(\tau_{12})_{ult}^2} \quad (18)$$

Failure theory components not directly derivable from the five laminate strength parameters. Those must be calibrated for  $H_{12}$  using empirical methods, such as the Hoffman criterion.

$$H_{12} = -\frac{1}{2(\sigma_1^T)_{ult}(\sigma_1^C)_{ult}} \quad (19)$$

The Norris-McKinnon criterion is a quadratic failure theory that is considered one of the first and simplest approaches for analyzing composite failure. This criterion evaluates whether a specified

level of stress would result in failure by considering the material's tensile, compressive, and shear strengths.

$$\left(\frac{\sigma_x}{(\sigma_x)_{ult}}\right)^2 + \left(\frac{\sigma_y}{(\sigma_y)_{ult}}\right)^2 + \left(\frac{\tau_{xy}}{(\tau_{xy})_{ult}}\right)^2 = 1 \quad (20)$$

A comparative analysis of the fatigue life characteristics of flax fibre and glass fibre reinforced epoxy composites was undertaken, utilizing two distinct fibre orientations of  $\pm 45^\circ$  and  $0^\circ/90^\circ$ . Composites reinforced with flax fibers oriented at  $0^\circ/90^\circ$  showed a lower fatigue endurance than glass fibers. Although epoxy composites reinforced with  $\pm 45^\circ$  flax fibers had a comparable fatigue endurance to those made with glass fibers in the high-cycle region [42], angle of  $\pm 45^\circ$  does not offer superior strength in either the x or y direction compared to an angle of  $0^\circ/90^\circ$  in laminate. Previous investigations had established that a quasi-isotropic laminate Ramir-PLA configuration endured 894,052 cycles when subjected to 55% of its ultimate strength [36]. Owing to the availability of this empirical data, the present study adopts the quasi-isotropic laminate [ $0^\circ/90^\circ/\pm 45^\circ$ ] configuration for the prosthetic foot.

Due to the study limitations, the fatigue test results could not be characterized. A model employing random hemp fibers with quasi-isotropic properties approximated fatigue cycles. These results informed the development of the material's fatigue failure criterion equation as follows:

$$S_m = 1 - \eta \ln(N) \quad (21)$$

Where N is the number of fatigue life cycles to failure,  $S_m$  is the new modified stress level. The fatigue sensitivity index ( $\eta$ ) was found to be 0.0517 using best-fit linear regression; the R2-value of 0.99 indicated a strong correlation with the data, signifying a good fit based on the experimental data [43].

$$S_m = \frac{\sigma_m}{\sigma_{ut} - \sigma_a} \quad (22)$$

Where  $\sigma_m$  is the mean stress,  $\sigma_a$  is the fatigue stress amplitude and  $\sigma_{ut}$  is ultimate tensile strength. Using the given equation and a 10% fatigue stress ratio, the resulting cycle value is equivalent to  $10^6$ , which corresponds to 42.1%  $\sigma_{ut}$  material. Additionally, other sources suggest that the maximum working stress is typically set between 25% and 40 % of  $\sigma_{ut}$  [10], [44], [45]. However, for composite materials with a defined fatigue limit, the fatigue resistance under compressive loading is typically higher than under tensile loading.

The exact percentage difference varies by material, but the compressive fatigue limit is commonly 10–20% higher than the tensile fatigue limit. If expressed as a fraction of the respective ultimate strengths, the compressive fatigue limit typically ranges between 50% and 65% of the ultimate compressive strength, whereas the tensile fatigue limit is only 40–55% of the ultimate tensile strength [43], [46], [47]. Therefore, the same equation utilised in the compression zone is used to predict the fatigue line.

### 2.3 Prosthetic production

The prosthetic foot prototype was fabricated using the hot press method, following a process similar to that used in the lamina characterization stage. The ramie fiber sheets were prepared in quasi-isotropic layup configurations: 54 layers (upper foot segment) and 32 layers (lower foot segment). The composite prepreg ramie fiber materials were prepared in dimensions of 250 mm × 100 mm

(upper segment) and 150 mm × 100 mm (lower segment). The orientation followed a sequence of  $[0^\circ/90^\circ/\pm 45^\circ]$  to ensure quasi-isotropic mechanical properties in the laminate structure. The molding apparatus used for fabrication consisted of aluminum molds shaped according to the anatomical geometry of a prosthetic foot. A release fabric was applied to each mold surface to facilitate easy removal of the cured laminate. The composite layups were compressed under a temperature of 110 °C and pressure of 132 bar for approximately 90 minutes. After hot pressing, the composite panels were trimmed to final shape using precision laser cutting.

The assembly consisted of joining the upper and lower foot segments using mechanical fasteners complemented by structural adhesives. This ensured robust bonding between the sole and aluminum connectors. The finalized prototype was subsequently prepared for static and dynamic mechanical testing.

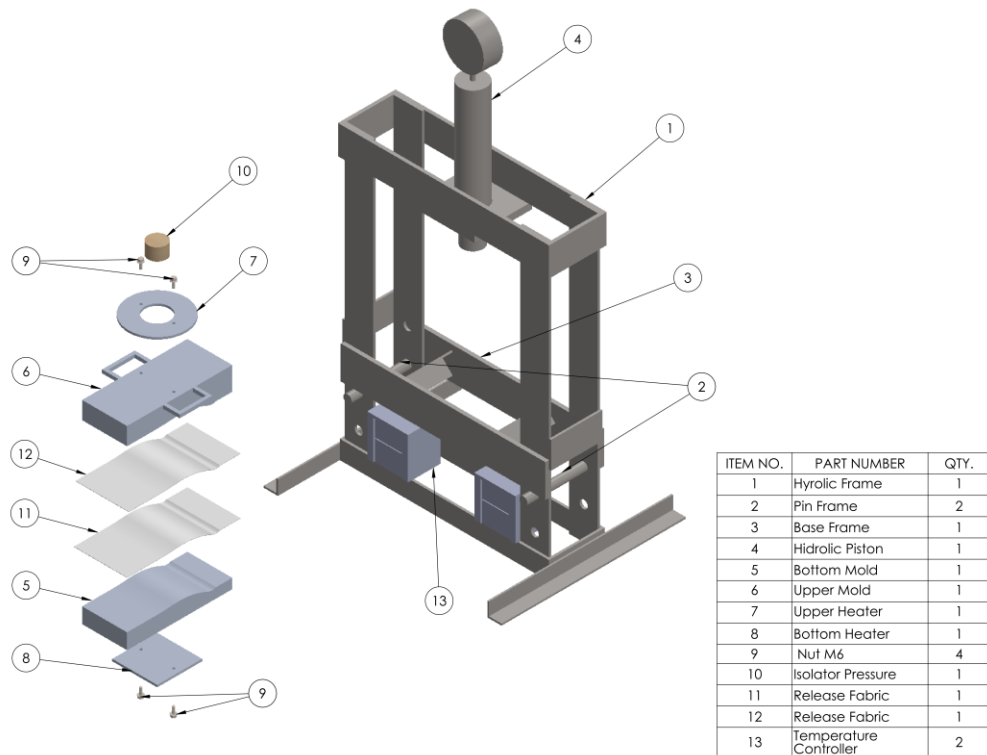


**Figure 2.** Ramie-PLA hot press setup

## 2.4 Prosthetic static test

The final prosthetic foot prototype was subjected to various static testing procedures to evaluate its performance before the dynamic test. The testing setup and procedures were designed to mimic the anticipated loading conditions during the gait cycle, including the heel strike and toe-off phases. Strain gages were strategically placed on multiple surfaces of the prosthetic foot to measure the normal stresses during the static tests. The prosthetic foot was subjected to non-destructive compressive load testing. These loading conditions aligned with the finite element simulation results, which were derived from the gait analysis data. The testing covered the heel strike and toe-off phases of the step cycle [39], [41], [48]. During the heel strike phase, a 15° angle was applied with a 780 N force. In the toe-off phase, a 20° angle was applied with a 715 N force. The experimental setup is shown in Figure 3. The Tensilon UTM RTG-1250 machine was employed to obtain a static test with 10 kN load cell.

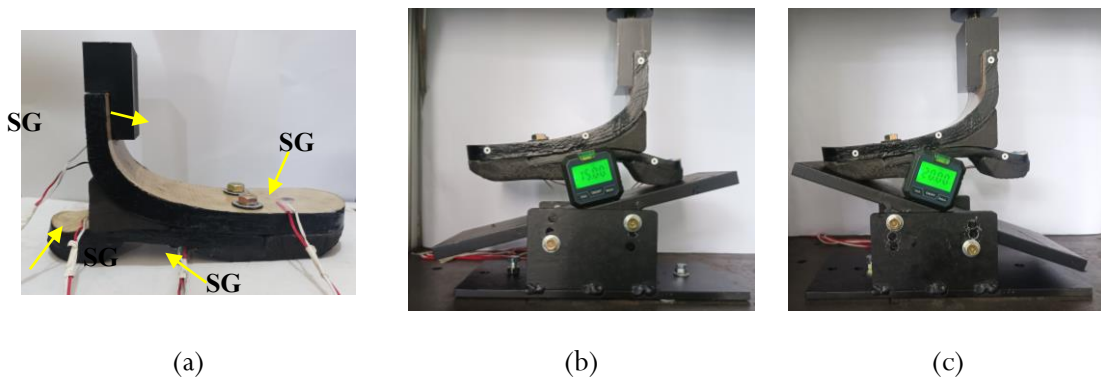


**Figure 3.** Strain gauges and cycle test position, (a) Strain gauges location, (b) Heel strike position setup, (c) Toe-off position setup

Strain gauges (SG) were used to record normal strain in material testing and analysis, as shown in Figure 3 (a). Strain gauges were installed at four positions to monitor operational stresses and verify compliance with allowable stress limits. The measured values were then compared with prior simulation results. Strain gauges data processing employ Hooke's Law equation, which relies on the elastic modulus derived from previous composite laminate testing. The static speed testing of the experiment was conducted at a rate of 3 mm/min.

$$\sigma = E \cdot \epsilon \quad (23)$$

### 3. Results and discussion

#### 3.1 Material and testing validation

The ramie-PLA composite test specimens were fabricated with a quasi-isotropic stacking sequence of  $[0^\circ/90^\circ/\pm 45^\circ]$ , resulting in an average thickness of  $14.69 \pm 0.03$  mm and a width of  $2.35 \pm 0.08$  mm. Tensile testing yielded an ultimate tensile strength of  $48.36 \pm 0.95$  MPa and an elastic modulus of  $4.125 \pm 0.25$  GPa. Statistical analysis using ANOVA at a significance level of  $\alpha = 0.05$  indicated no significant difference in tensile strength ( $p = 0.99$ ), but a significant difference was observed in the elastic modulus ( $p = 0.002$ ). Therefore, the experimental modulus was applied in subsequent stress analysis based on strain gauge data. Table 2 summarizes the experimentally determined mechanical properties of EVA cushioning material, whereas Table 3 provides a comparison between the theoretical prediction and experimental measurements for the ramie-PLA composite laminate.

**Table 2.** Experimental mechanical properties of EVA

Properties	Experimental value	Unit
$\sigma_{ult}$	$1.049 \pm 0.08$	MPa
E	$2.36 \pm 0.19$	MPa
$\epsilon_{ult}$	$167.82\% \pm 18\%$	m/m

Flexural testing of the composite specimens, which had an average thickness of  $4.8 \pm 0.15$  mm and width of  $12.73 \pm 0.02$  mm, yielded a maximum flexural stress of  $62.06 \pm 3.43$  MPa over a span of 114 mm (Figure 4). The obtained flexural and tensile properties define the mechanical performance boundaries for the design and evaluation of prosthetic foot prototype.

**Table 3.** Theoretical predictions and experimental measurements for ramie-PLA

Properties	Theoretical predictions	Experimental measurements	Unit
$(\sigma_x^T)_{ult}$	48.38	$48.36 \pm 0.95$	MPa
$(\sigma_y^T)_{ult}$	48.38	$48.36 \pm 0.95$	MPa
$E_1$	4.67	$4.125 \pm 0.25$	GPa
$E_2$	4.67	$4.125 \pm 0.25$	GPa

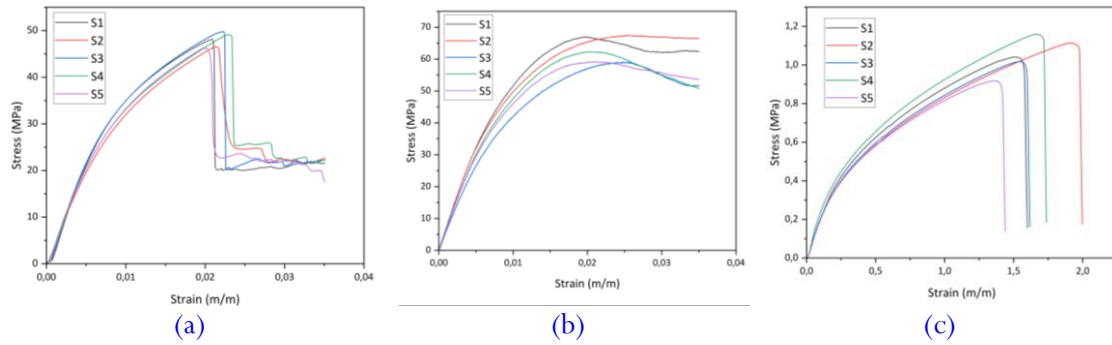


**Figure 4.** Mechanical properties result, (a) Laminate tensile test, (b) Laminate flexural test, (c) EVA tensile test

Figure 5 displays the fracture morphology of a ramie fiber-reinforced PLA composite following standard tensile testing. Results from microscopic examination indicate that the main causes of failure involve interfacial debonding and uneven fibre fracture. The weak adhesion between ramie fibers and the PLA matrix leads to ineffective load transfer under tensile stress, indicating suboptimal composite performance. At higher SEM magnification, the visible gaps between fibers indicate adhesive failure. The observed debonding and delamination phenomenon indicates that the fibers are more likely to separate from the matrix before fracturing. This suggests a significant portion of the energy absorbed during deformation is released through fiber-matrix separation rather than fiber fracture.

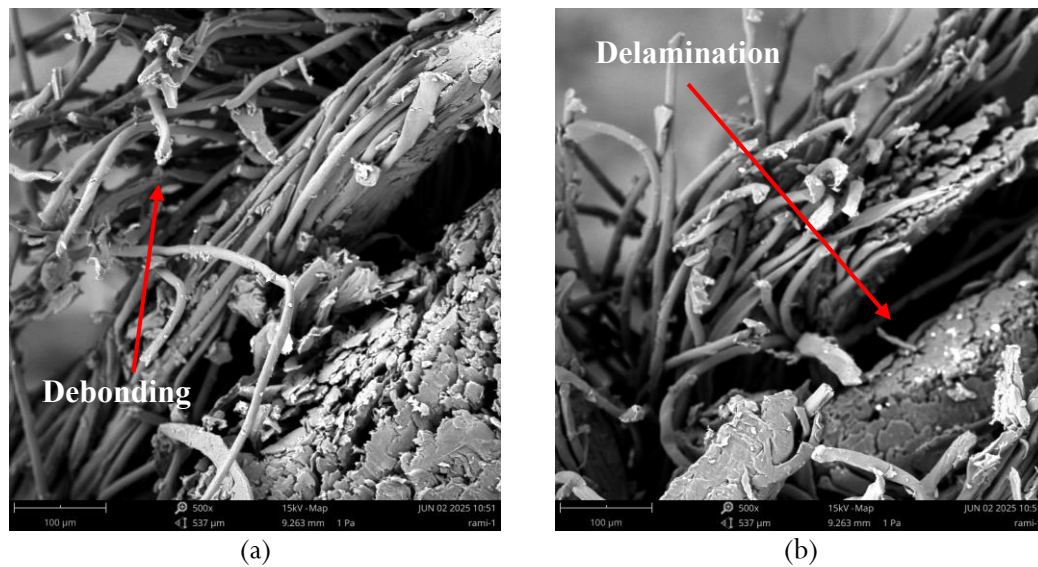


**Figure 5.** Fracture in ramie-PLA tension test with SEM magnification, (a) Debonding, (b) Delamination

### 3.2 Design and analysis

The prosthetic foot was designed to meet dynamic performance requirements during walking, particularly during heel strike and toe-off phases. The minimum thickness required for the laminate structure was determined based on the dynamic tensile strength and quasi-isotropic configuration of the ramie-PLA composite. The calculated minimum thicknesses were 11.2 mm for heel-strike and 18.2 mm for toe-off conditions. With a single layer thickness of 0.35 mm, this aligns to 32 layers for the heel segment and 52 layers for the toe-off segment. The stress limits based on the fatigue criterion were  $(\sigma_x^T)_{fg} = 20.36$  MPa,  $(\sigma_y^T)_{fg} = 20.36$  MPa,  $(\tau_{xy})_{fg} = 14.36$  MPa,  $(\sigma_x^C)_{fg} = 16.19$  MPa, &  $(\sigma_y^C)_{fg} = 16.19$  MPa.

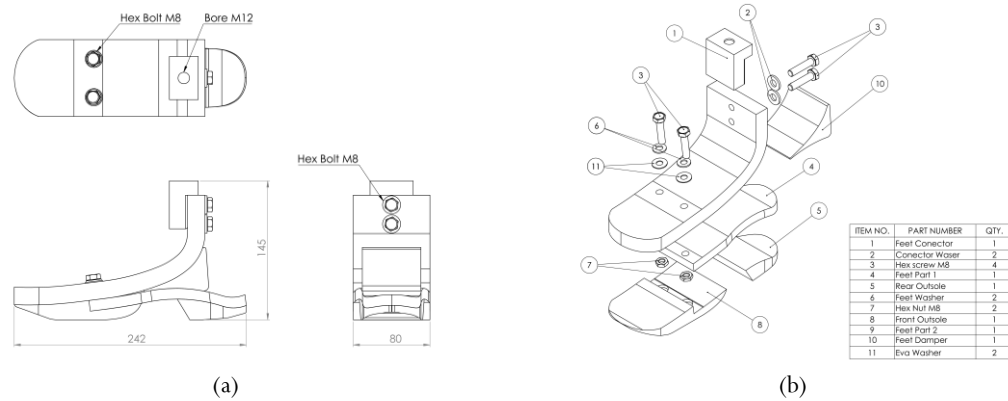


**Figure 6.** Design of prosthetic foot, (a) 3D Model of prosthetic foot, (b) Exploded view of prosthetic foot

The finite element analysis model uses an optimized mesh with an element size of 2 mm to model the prosthetic foot design. Figure 7 and Figure 8 illustrate the loading, stress distributions, and deformation results for both gait phases. The simulation results showed compressive normal stresses of -11.44 MPa to +17.78 MPa (heel strike phase) and -12.28 MPa to +12.38 MPa (toe-off phase). All these values remained within the fatigue stress threshold. Shear stress values ranged from -2.37 MPa to +1.71 MPa during heel strike, and from -6.96 MPa to +5.69 MPa during toe-off. All values remained within safe limits.

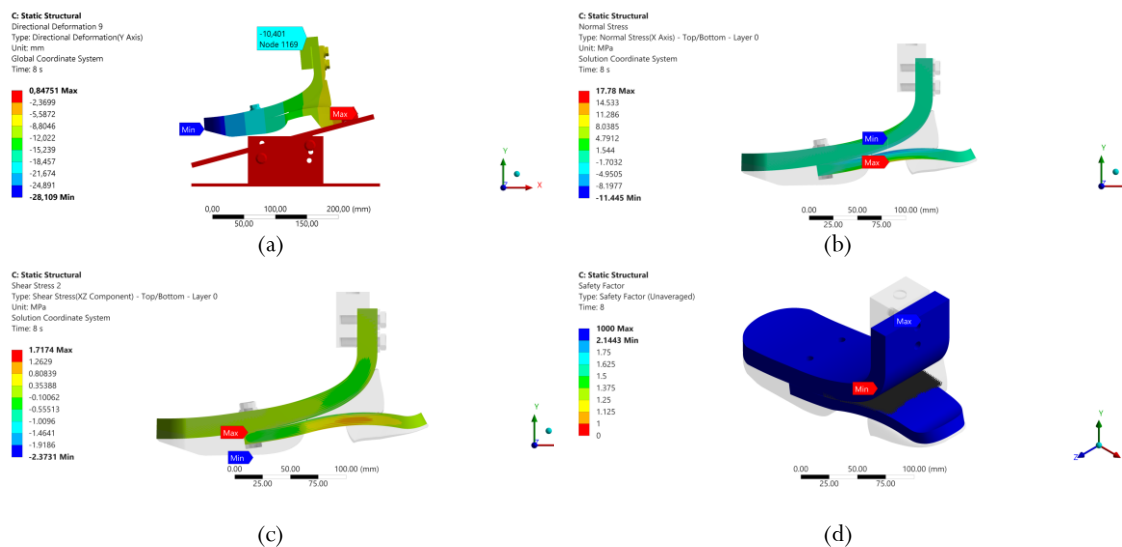


**Figure 7.** FEM Analysis in heel strike phase, (a) Force apply, (b) Normal stress, (c) Shear stress, (d) Total deformation

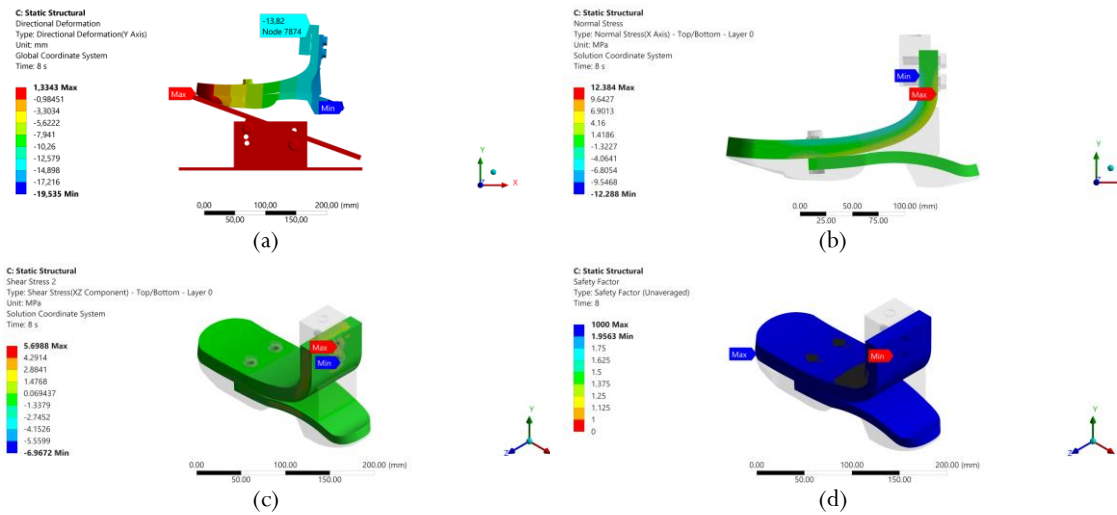


**Figure 8.** FEM Analysis in Toe-Off Phase, (a) Force apply, (b) Normal stress, (c) Shear stress, (d) Total deformation

Connector deformation analysis indicated deflections of  $-10.4$  mm in heel strike and  $-13.82$  mm in toe-off, consistent with expected displacements during gait. To further validate structural safety, the Tsai-Wu and Norris–McKinnon failure criteria were applied using the stress values obtained from the FEA. Multiaxial stress nodes were plotted onto the failure envelope Figure 9, which confirmed that the proposed laminate structure avoids critical fracture and fatigue zones.

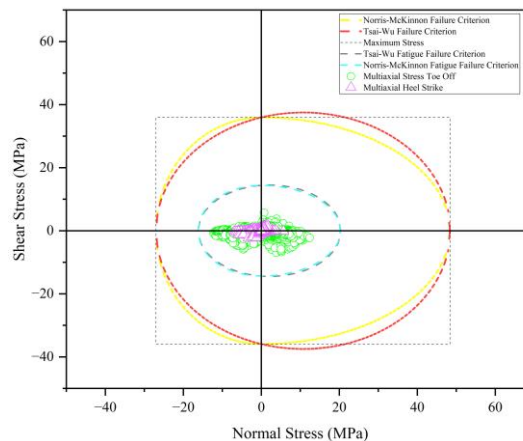


**Figure 9.** Multiaxial node stress result on failure envelope

These simulation results confirm that the prosthetic foot design, employing ramie-PLA composite with a quasi-isotropic layup, satisfies dynamic mechanical requirements for lower-limb prosthetics under repetitive gait loading conditions [49], [50], [51]. Utilizing normal and shear stress values obtained from the ANSYS analysis, a failure envelope was constructed based on the Tsai-Wu and Norris-McKinnon failure criteria to identify potential fracture and fatigue zones in the design. The failure analysis confirms that the proposed prosthetic foot design effectively avoids the failure fatigue zones. These ensure its structural integrity and reliability under all anticipated loading conditions.

### 3.3 Prosthetic production

The layup followed a  $[0^\circ/90^\circ/\pm 45^\circ]$  sequence to ensure quasi-isotropic mechanical behavior. Each segment was placed in a mold cavity shaped to match the anatomical contour of a transtibial prosthetic foot. A release fabric was applied to the mold surfaces to facilitate easy removal of the

cured laminate. Figure 10 displays the main manufacturing steps, including the hot press molding and laser cutting processes.

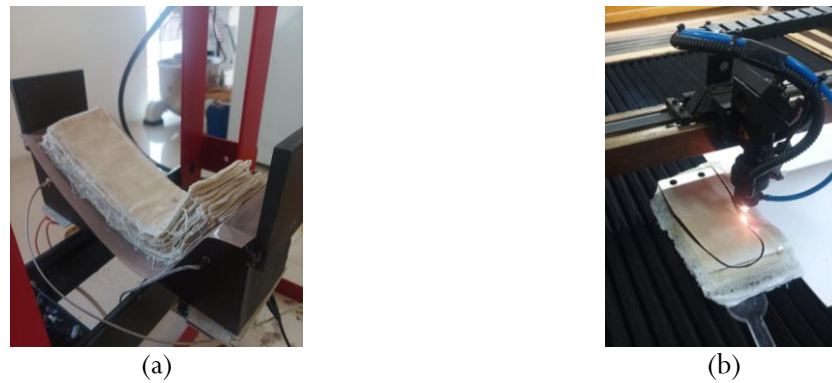


**Figure 10.** Manufacturing process of prosthetic foot, (a) Hot press process, (b) Laser cutting process

### 3.4 Prosthetic static result

The results indicated that the maximum measured stress values remained within acceptable limits in ANSYS finite element analysis, verifying the structural integrity of the prosthetic foot design. The displacement was also measured by the testing machine and compared to the design results.

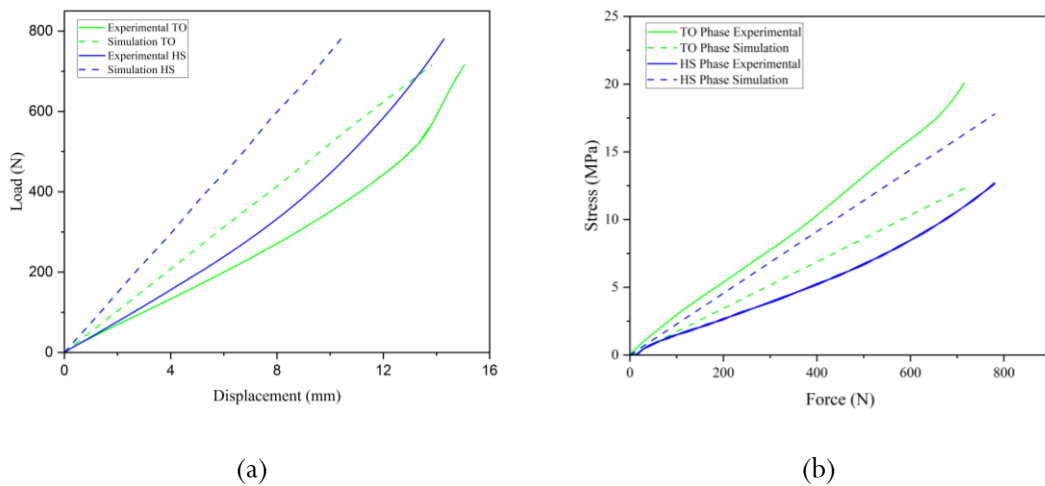


**Figure 11.** Simulation and experimental, (a) Displacement of prosthetic Foot, (b) Maximum stress of prosthetic foot

The comparison of actual deflection and the simulation data reveals critical insights into the accuracy and reliability of the computational model (Figure 11). The simulation data indicated a lower deflection value compared to the experimental test results. The graph shows that the actual deflection values were greater than the simulated values. Specifically, for the toe-off condition, the actual deflection was 15.04 mm, while the simulated deflection was 13.81 mm. Similarly, for the heel strike condition, the actual deflection was 14.28 mm, whereas the simulated deflection was 10.4 mm. The observed discrepancy between the simulation data and experimental results can be attributed to several factors. Those factors are simplifications in the calculation of laminate material properties within the simulation model, potential differences in boundary conditions between the idealized computational model and the physical test setup, as well as the inherent limitations of finite element analysis in accurately capturing the complex mechanical behavior of composite structures. The comparison of the actual stress measurements and the simulation data underscores

the fidelity and predictive capability of the computational modeling approach utilized in this investigation.

The comparison of actual stress measurements and the simulation data reveals differences in the stress values. In particular, the actual maximum stress during the heel strike phase was 12.72 MPa at the surface of the strain gauge 3, while the simulated value was 17.78 MPa. Similarly, for the toe-off phase, the actual stress was 20.09 MPa at the surface of the strain gauge 1, whereas the simulated stress was 12.38 MPa. The observed discrepancies between experimental and simulated stress likely stem from simplifications in the material modeling, idealized boundary conditions, and inherent limitations of finite element methods in capturing the complex behavior of composites. The static testing results demonstrated that the actual stress measurements were within the acceptable fatigue stress limits, thereby validating the structural integrity of the prosthetic foot prototype.

#### 4. Conclusion

This study designed, developed, and experimentally evaluated a sustainable ramie fiber/PLA composite prosthetic foot prototype fabricated via hot press prepreg. The composite demonstrated suitable mechanical properties for prosthetic applications. The observed variations between ANSYS simulations and experimental data from inherent differences between idealized computational models and physical testing environments. Specifically, computer simulations rely on perfect geometries, boundary conditions, and uniform material properties. Unlike simulation, experimental testing introduces measurable variations inherent to physical systems. One contributing factor is the manufacturing process of the prosthetic foot; slight inconsistencies in fiber alignment, layer thickness, and PLA distribution create local differences in stiffness and stress response. These variations are difficult to replicate exactly in the model, resulting in some discrepancy between predicted and observed behavior. Furthermore, the physical test setup itself can contribute to differences. Fixture tolerances, imperfect clamping, and alignment errors may affect the application and distribution of load. In certain cases, slippage at the support interfaces, particularly during high-strain phases (heel strike or toe-off), can absorb part of the load. Thus, reducing measured stress values. Friction, minor lateral movement, and flexibility in the test apparatus are further sources of deviation not typically captured in simulation. Finite element analysis using a quasi-isotropic lamina lay-up validated the design. It confirms that all stresses under simulated gait phases remained within fatigue limit thresholds, as well as the static testing results. The experimental stress measurements align closely with simulation predictions. These remained below the fatigue stress limit, confirming the mechanical integrity of the structure under load. The ramie-PLA composite prosthetic foot prototype exhibits significant promise as a sustainable and economically viable solution for individuals with lower-limb amputations, particularly in resource-constrained environments.

Building upon the encouraging outcomes of static testing, future studies will prioritize dynamic and fatigue *in vitro* assessments to evaluate the prototype's long-term resilience under cyclical loading conditions. These evaluations are designed to replicate real-world usage patterns and ensure sustained mechanical reliability. Furthermore, future investigations will examine enhancements in ergonomic design and gait performance to optimize user comfort and functionality. Clinical studies involving amputee subjects are scheduled to assess safety, performance, and user satisfaction in authentic settings. These measurements are crucial for validating the prototype's efficacy beyond controlled laboratory conditions and aligning its development with real-world needs. With its cost-effective and biodegradable material composition, this prosthetic model offers a compelling alternative to conventional designs. To foster widespread impact, the research team will perform cost-benefit analyses, engage with local prosthetic manufacturers, and establish partnerships with NGOs and healthcare networks. These initiatives aim to facilitate commercialization, clinical

integration, and extensive distribution, particularly for marginalized populations. These solidify the study's significance and societal contribution.

### Author's declaration

### Author contribution

**Iyan Sopiyan:** methodology, validation, formal analysis, finite element analysis, material preparation, investigation, resources, writing – original draft. **Tresna P. Soemardi:** conceptualization, supervision. **Herry Purnomo:** material preparation, validation support, resources, investigation. **Olivier Polit:** finite element analysis, methodology review, formal analysis.

### Funding statement

This research was funded by the Indonesia Endowment Fund for Education (Lembaga Pengelola Dana Pendidikan – LPDP), Ministry of Finance of the Republic of Indonesia. The authors gratefully acknowledge the financial support provided through the LPDP scholarship program, which enabled the completion and publication of this work.

### Data Availability

The raw data of this study is available. If anyone wishes to use it as a basis for further research, please contact the corresponding author.

### Acknowledgements

The authors would like to express their sincere gratitude to the Indonesia Endowment Fund for Education (Lembaga Pengelola Dana Pendidikan – LPDP), Ministry of Finance of the Republic of Indonesia, for providing the financial support through the LPDP scholarship program.

### Competing interest

The authors declare no known competing financial interests or personal relationships that could have appeared to influence the work reported in this paper.

### Ethical clearance

This research does not involve humans as subjects.

### AI statement

The grammatical structure of this article was improved using Trinkai.ai through institutional access, and the authors have rechecked the accuracy and correctness with the topic and data of this study.

### Publisher's and Journal's note

Universitas Negeri Padang as the publisher, and Editor of Teknomekanik state that there is no conflict of interest towards this article publication.

## References

- [1] S.-C. Shi, S.-T. Cheng, and D. Rahmadiawan, "Developing biomimetic PVA/PAA hydrogels with cellulose nanocrystals inspired by tree frog structures for superior wearable sensor functionality," *Sens Actuators A Phys*, vol. 379, p. 115981, Dec. 2024, <https://doi.org/10.1016/j.sna.2024.115981>
- [2] S.-C. Shi, S.-W. Ouyang, and D. Rahmadiawan, "Erythrosine–Dialdehyde Cellulose Nanocrystal Coatings for Antibacterial Paper Packaging," *Polymers (Basel)*, vol. 16, no. 7, p. 960, Apr. 2024, <https://doi.org/10.3390/polym16070960>
- [3] M. Ibadi, H. Purnomo, D. N. Vicarneltor, H. B. Wibowo, M. H. Setianto, and Y. Whulanza, "Investigation of Thermomechanical Analysis of Carbon/Epoxy Composite for Spacecraft Structure Material," *Sains Malays*, vol. 53, no. 3, pp. 691–704, Mar. 2024, <https://doi.org/10.17576/jsm-2024-5303-16>
- [4] L. Nolan, "Carbon fibre prostheses and running in amputees: A review," *Foot and Ankle Surgery*, vol. 14, no. 3, pp. 125–129, Jan. 2008, <https://doi.org/10.1016/j.fas.2008.05.007>
- [5] Y. Lian *et al.*, "Multifunctional electromagnetic wave absorbing carbon fiber/Ti3C2TX MXene fabric with superior near-infrared laser dependent photothermal antibacterial behaviors," *J Colloid Interface Sci*, vol. 676, pp. 217–226, Dec. 2024, <https://doi.org/10.1016/j.jcis.2024.07.102>
- [6] T. P. Soemardi, O. Polit, F. Salsabila, and A. Lololau, "Ramie Fiber-Reinforced Polylactic-Acid Prepreg: Fabrication and Characterization of Unidirectional and Bidirectional Laminates," *International Journal of Technology*, vol. 14, no. 4, p. 888, Jun. 2023, <https://doi.org/10.14716/ijtech.v14i4.5940>
- [7] K. Matsumoto, K. Takemura, R. Kitamura, H. Katogi, T. Tanaka, and H. Takagi, "Cellulose nanofiber-introduced continuous-ramie yarn-reinforced polylactic acid filament for 3D printing: Novel fabrication process and mechanical properties," *Compos Part A Appl Sci Manuf*, vol. 176, p. 107836, Jan. 2024, <https://doi.org/10.1016/j.compositesa.2023.107836>
- [8] M. J. John, K. T. Varughese, and S. Thomas, "Green Composites from Natural Fibers and Natural Rubber: Effect of Fiber Ratio on Mechanical and Swelling Characteristics," *Journal of Natural Fibers*, vol. 5, no. 1, pp. 47–60, Apr. 2008, <https://doi.org/10.1080/15440470801901480>
- [9] S. D. Varsavas and C. Kaynak, "Weathering degradation performance of PLA and its glass fiber reinforced composite," *Mater Today Commun*, vol. 15, pp. 344–353, Jun. 2018, <https://doi.org/10.1016/j.mtcomm.2017.11.008>
- [10] A. Lololau, T. P. Soemardi, H. Purnama, and O. Polit, "Composite Multiaxial Mechanics: Laminate Design Optimization of Taper-Less Wind Turbine Blades with Ramie Fiber-Reinforced Polylactic Acid," *International Journal of Technology*, vol. 12, no. 6, p. 1273, Dec. 2021, <https://doi.org/10.14716/ijtech.v12i6.5199>
- [11] A. D. Shieddieque, M. Mardiyati, R. Suratman, and B. Widyanto, "Preparation and Characterization of Sansevieria trifasciata Fiber/High-Impact Polypropylene and Sansevieria trifasciata Fiber/Vinyl Ester Biocomposites for Automotive Applications," *International Journal of Technology*, vol. 12, no. 3, p. 549, Jul. 2021, <https://doi.org/10.14716/ijtech.v12i3.2841>
- [12] Y. Wu *et al.*, "Green and sustainable bamboo based composites with high self-bonding strength," *Compos B Eng*, vol. 287, p. 111849, Dec. 2024, <https://doi.org/10.1016/j.compositesb.2024.111849>
- [13] Z. Yu *et al.*, "Green and sustainable metal-reinforced bamboo composites with high self-bonding performances," *Ind Crops Prod*, vol. 223, p. 120053, Jan. 2025, <https://doi.org/10.1016/j.indcrop.2024.120053>

- [14] R. Siakeng, M. Jawaid, H. Ariffin, S. M. Sapuan, M. Asim, and N. Saba, "Natural fiber reinforced polylactic acid composites: A review," *Polym Compos*, vol. 40, no. 2, pp. 446–463, Feb. 2019, <https://doi.org/10.1002/pc.24747>
- [15] S. Sharma, A. Majumdar, and B. S. Butola, "Tailoring the biodegradability of polylactic acid (PLA) based films and ramie- PLA green composites by using selective additives," *Int J Biol Macromol*, vol. 181, pp. 1092–1103, Jun. 2021, <https://doi.org/10.1016/j.ijbiomac.2021.04.108>
- [16] T. Yu, C. Hu, X. Chen, and Y. Li, "Effect of diisocyanates as compatibilizer on the properties of ramie/poly(lactic acid) (PLA) composites," *Compos Part A Appl Sci Manuf*, vol. 76, pp. 20–27, Sep. 2015, <https://doi.org/10.1016/j.compositesa.2015.05.010>
- [17] K. Shimoda and H. Kakisawa, "Novel production route for SiC/SiC ceramic-matrix composites using sandwich prepreg sheets," *J Eur Ceram Soc*, vol. 43, no. 3, pp. 805–813, Mar. 2023, <https://doi.org/10.1016/j.jeurceramsoc.2022.11.005>
- [18] M. Omasta, D. Paloušek, T. Návrát, and J. Rosický, "Finite element analysis for the evaluation of the structural behaviour, of a prosthesis for trans-tibial amputees," *Med Eng Phys*, vol. 34, no. 1, pp. 38–45, Jan. 2012, <https://doi.org/10.1016/j.medengphy.2011.06.014>
- [19] K. M. Cyr, R. R. Neptune, and G. K. Klute, "Influence of prosthetic foot selection on walking performance during various load carriage conditions," *Clinical Biomechanics*, vol. 122, p. 106440, Feb. 2025, <https://doi.org/10.1016/j.clinbiomech.2025.106440>
- [20] A. Eshraghi, Z. Safaeepour, M. D. Geil, and J. Andrysek, "Walking and balance in children and adolescents with lower-limb amputation: A review of literature," *Clinical Biomechanics*, vol. 59, pp. 181–198, Nov. 2018, <https://doi.org/10.1016/j.clinbiomech.2018.09.017>
- [21] H. Hobara, H. Sakata, S. Hashizume, and Y. Kobayashi, "Leg stiffness in unilateral transfemoral amputees across a range of running speeds," *J Biomech*, vol. 84, pp. 67–72, Feb. 2019, <https://doi.org/10.1016/j.jbiomech.2018.12.014>
- [22] O. N. Beck, P. Taboga, and A. M. Grabowski, "Characterizing the Mechanical Properties of Running-Specific Prostheses," *PLoS One*, vol. 11, no. 12, p. e0168298, Dec. 2016, <https://doi.org/10.1371/journal.pone.0168298>
- [23] F. S. Prome, M. F. Hossain, M. S. Rana, M. M. Islam, and M. S. Ferdous, "Different chemical treatments of natural fiber composites and their impact on water absorption behavior and mechanical strength," *Hybrid Advances*, vol. 8, p. 100379, Mar. 2025, <https://doi.org/10.1016/j.hybadv.2025.100379>
- [24] S. Alazzawi, W. A. Mahmood, and S. K. Shihab, "Comparative study of natural fiber-Reinforced composites for sustainable thermal insulation in construction," *International Journal of Thermofluids*, vol. 24, p. 100839, Nov. 2024, <https://doi.org/10.1016/j.ijft.2024.100839>
- [25] R. Versluys, P. Beyl, M. Van Damme, A. Desomer, R. Van Ham, and D. Lefebber, "Prosthetic feet: State-of-the-art review and the importance of mimicking human ankle-foot biomechanics," *Disabil Rehabil Assist Technol*, vol. 4, no. 2, pp. 65–75, Jan. 2009, <https://doi.org/10.1080/17483100802715092>
- [26] J. K. Burnett, Y. T. Choi, H. Li, N. M. Wereley, R. H. Miller, and J. K. Shim, "Vibration Suppression of a Composite Prosthetic Foot Using Piezoelectric Shunt Damping: Implications to Vibration-Induced Cumulative Trauma," *IEEE Trans Biomed Eng*, vol. 68, no. 9, pp. 2741–2751, Sep. 2021, <https://doi.org/10.1109/TBME.2021.3053374>
- [27] L. Zhu *et al.*, "Aging performance and mechanism of carbon fiber-reinforced bismaleamide composites under natural aging in marine environments," *Mater Today Commun*, vol. 41, p. 110796, Dec. 2024, <https://doi.org/10.1016/j.mtcomm.2024.110796>
- [28] S. Chandra Dubey, V. Mishra, and A. Sharma, "A review on polymer composite with waste material as reinforcement," *Mater Today Proc*, vol. 47, pp. 2846–2851, 2021, <https://doi.org/10.1016/j.matpr.2021.03.611>

- [29] V. Prost, W. B. Johnson, J. A. Kent, M. J. Major, and A. G. Winter, “Biomechanical evaluation over level ground walking of user-specific prosthetic feet designed using the lower leg trajectory error framework,” *Sci Rep*, vol. 12, no. 1, p. 5306, Mar. 2022, <https://doi.org/10.1038/s41598-022-09114-y>
- [30] C. P. McGowan, A. M. Grabowski, W. J. McDermott, H. M. Herr, and R. Kram, “Leg stiffness of sprinters using running-specific prostheses,” *J R Soc Interface*, vol. 9, no. 73, pp. 1975–1982, Aug. 2012, <https://doi.org/10.1098/rsif.2011.0877>
- [31] D. Xu *et al.*, “A new method proposed for realizing human gait pattern recognition: Inspirations for the application of sports and clinical gait analysis,” *Gait Posture*, vol. 107, pp. 293–305, Jan. 2024, <https://doi.org/10.1016/j.gaitpost.2023.10.019>
- [32] C. L. McDonald, P. A. Kramer, S. J. Morgan, E. G. Halsne, S. M. Cheever, and B. J. Hafner, “Energy expenditure in people with transtibial amputation walking with crossover and energy storing prosthetic feet: A randomized within-subject study,” *Gait Posture*, vol. 62, pp. 349–354, May 2018, <https://doi.org/10.1016/j.gaitpost.2018.03.040>
- [33] L. Sedran *et al.*, “Quantification of push-off and collision work during step-to-step transition in amputees walking at self-selected speed: Effect of amputation level,” *J Biomech*, vol. 163, p. 111943, Jan. 2024, <https://doi.org/10.1016/j.jbiomech.2024.111943>
- [34] R. Matter, M. Harniss, T. Oderud, J. Borg, and A. H. Eide, “Assistive technology in resource-limited environments: a scoping review,” *Disabil Rehabil Assist Technol*, vol. 12, no. 2, pp. 105–114, Feb. 2017, <https://doi.org/10.1080/17483107.2016.1188170>
- [35] M. van der Stelt *et al.*, “Pioneering low-cost 3D-printed transtibial prosthetics to serve a rural population in Sierra Leone – an observational cohort study,” *EClinicalMedicine*, vol. 35, p. 100874, May 2021, <https://doi.org/10.1016/j.eclinm.2021.100874>
- [36] Ardy Lefran Lololau, “Ramie Fiber-Reinforced Polylactic-Acid Composite Prepreg: The Engineering And The Characterization of Its Mechanical Multiaxial Behavior,” Universitas Indonesia, Depok, 2024.
- [37] A. Saveko *et al.*, “Foot-ground reaction force during long-term space flight and after it: walking in active treadmill mode,” *Gait Posture*, vol. 76, pp. 382–388, Feb. 2020, <https://doi.org/10.1016/j.gaitpost.2019.12.033>
- [38] M. Künzler, S. Herger, E. De Pieri, C. Egloff, A. Mündermann, and C. Nüesch, “Effect of load carriage on joint kinematics, vertical ground reaction force and muscle activity: Treadmill versus overground walking,” *Gait Posture*, vol. 104, pp. 1–8, Jul. 2023, <https://doi.org/10.1016/j.gaitpost.2023.05.018>
- [39] A. R. N. Al Thahabi *et al.*, “Numerical design and experimental validation of a 3D-printed composite energy-storage-and-return prosthetic foot,” *Compos Struct*, vol. 358, p. 118907, Mar. 2025, <https://doi.org/10.1016/j.compstruct.2025.118907>
- [40] M. Perkasa *et al.*, “Composite Mechanics Simulation for Design of a Lower Limb Prosthetic using Ramie Fiber-Reinforced Polylactic-Acid Composite,” *International Journal of Technology*, vol. 16, no. 2, p. 470, Mar. 2025, <https://doi.org/10.14716/ijtech.v16i2.7363>
- [41] G. I. Lopez-Avina, E. Barocio, and J. C. Huegel, “Pseudo fatigue test of passive energy-returning prosthetic foot,” in *2017 IEEE Global Humanitarian Technology Conference (GHTC)*, IEEE, Oct. 2017, pp. 1–7. <https://doi.org/10.1109/GHTC.2017.8239315>
- [42] N. L. Feng, S. D. Malingam, R. Jenal, Z. Mustafa, and S. Subramonian, “A review of the tensile and fatigue responses of cellulosic fibre-reinforced polymer composites,” *Mechanics of Advanced Materials and Structures*, vol. 27, no. 8, pp. 645–660, Apr. 2020, <https://doi.org/10.1080/15376494.2018.1489086>
- [43] A. Fotouh, J. D. Wolodko, and M. G. Lipsett, “Fatigue of natural fiber thermoplastic composites,” *Compos B Eng*, vol. 62, pp. 175–182, Jun. 2014, <https://doi.org/10.1016/j.compositesb.2014.02.023>
- [44] U. A. Mortensen, S. Rasmussen, L. P. Mikkelsen, A. Fraisse, and T. L. Andersen, “The impact of the fiber volume fraction on the fatigue performance of glass fiber composites,”

- Compos Part A Appl Sci Manuf*, vol. 169, p. 107493, Jun. 2023, <https://doi.org/10.1016/j.compositesa.2023.107493>
- [45] S. Asgarinia *et al.*, “Tension–tension fatigue behaviour of woven flax/epoxy composites,” *Journal of Reinforced Plastics and Composites*, vol. 34, no. 11, pp. 857–867, Jun. 2015, <https://doi.org/10.1177/0731684415581527>
- [46] S. Manteghi, A. Sarwar, Z. Fawaz, R. Zdero, and H. Bougherara, “Mechanical characterization of the static and fatigue compressive properties of a new glass/flax/epoxy composite material using digital image correlation, thermographic stress analysis, and conventional mechanical testing,” *Materials Science and Engineering: C*, vol. 99, pp. 940–950, Jun. 2019, <https://doi.org/10.1016/j.msec.2019.02.041>
- [47] B. Fazlali, S. V. Lomov, and Y. Swolfs, “Concerns in tension-tension fatigue testing of unidirectional composites: Specimen design and test setup,” *Compos B Eng*, vol. 272, p. 111213, Mar. 2024, <https://doi.org/10.1016/j.compositesb.2024.111213>
- [48] F. Starker, F. Blab, F. Dennerlein, and U. Schneider, “A Method for Sports Shoe Machinery Endurance Testing: Modification of ISO 22675 Prosthetic Foot Test Machine for Heel-to-toe Running Movement.,” *Procedia Eng*, vol. 72, pp. 405–410, 2014, <https://doi.org/10.1016/j.proeng.2014.06.072>
- [49] A. L. Pereira, M. D. Banea, J. S. S. Neto, and D. K. K. Cavalcanti, “Mechanical and Thermal Characterization of Natural Intralaminar Hybrid Composites Based on Sisal,” *Polymers (Basel)*, vol. 12, no. 4, p. 866, Apr. 2020, <https://doi.org/10.3390/polym12040866>
- [50] A. Porras and A. Maranon, “Development and characterization of a laminate composite material from polylactic acid (PLA) and woven bamboo fabric,” *Compos B Eng*, vol. 43, no. 7, pp. 2782–2788, Oct. 2012, <https://doi.org/10.1016/j.compositesb.2012.04.039>
- [51] A. Porras, A. Maranon, and I. A. Ashcroft, “Thermo-mechanical characterization of Manicaria Saccifera natural fabric reinforced poly-lactic acid composite lamina,” *Compos Part A Appl Sci Manuf*, vol. 81, pp. 105–110, Feb. 2016, <https://doi.org/10.1016/j.compositesa.2015.11.008>

## Nomenclature

Symbol	Description	Unit
$(\sigma_1^T)_{ult}$	= Ultimate tensile stress in the longitudinal (fiber) direction (1-direction)	MPa
$(\sigma_2^T)_{ult}$	= Ultimate tensile stress in the transverse direction (2-direction)	MPa
$(\tau_{12})_{ult}$	= Ultimate in-plane shear stress between the 1- and 2-directions of the composite	MPa
$(\sigma_1^C)_{ult}$	= Ultimate compressive stress in the longitudinal direction	MPa
$(\sigma_2^C)_{ult}$	= Ultimate compressive stress in the transverse direction	MPa
$(\sigma_x)_{ult}$	= Ultimate stress in the x-direction (global coordinate)	MPa
$(\sigma_y)_{ult}$	= Ultimate stress in the y-direction (global coordinate)	MPa
$(\tau_{xy})_{ult}$	= Ultimate shear stress in the xy-plane (global coordinate)	MPa
$E_1$	= Elastic modulus in the longitudinal direction	GPa
$E_2$	= Elastic modulus in the transverse direction	GPa
$G_{12}$	= In-plane shear modulus	GPa
$\nu_{12}$	= Major Poisson’s ratio, i.e., transverse strain due to longitudinal stress	-
$\sigma_x$	= Normal stress in the x-direction (global coordinate)	MPa
$\sigma_y$	= Normal stress in the y-direction (global coordinate)	MPa
$\tau_{xy}$	= Shear stress in the xy-plane (global coordinate)	MPa
$\theta$	= Fiber orientation angle with respect to the x-axis	°
$\cos \theta, \sin \theta$	= Cosine and sine of the fiber orientation angle $\theta$	°
$\sigma_{dn}$	= Dynamic Stress Criterion	MPa
$M$	= Bending moment applied to the beam	Nmm
$y$	= Distance from the neutral axis to the outermost fiber	mm

$I$	=	Second moment of area (moment of inertia) of the beam cross-section	$\text{mm}^4$
$B$	=	Width of the beam or specimen	$\text{mm}$
$H$	=	Height or thickness of the beam or specimen	$\text{mm}$
$h_{min}$	=	Minimum height required to resist the bending stress without failure	$\text{Mm}$
$H_1$	=	Linear coefficient related to tensile and compressive strength in the 1-direction	$\text{MPa}^{-1}$
$H_{11}$	=	Quadratic coefficient for the stress interaction in the 1-direction	$\text{MPa}^{-2}$
$H_2$	=	Linear coefficient related to tensile and compressive strength in the 2-direction	$\text{MPa}^{-1}$
$H_{22}$	=	Quadratic coefficient for the stress interaction in the 2-direction	$\text{MPa}^{-2}$
$H_6$	=	Linear coefficient for shear stress $\tau_{12}$ (often zero in symmetric cases)	$\text{MPa}^{-1}$
$H_{66}$	=	Quadratic coefficient for in-plane shear stress interaction	$\text{MPa}^{-2}$
$H_{12}$	=	Interaction coefficient between tensile and compressive stress in the 1-direction, typically used in quadratic failure criteria	$\text{MPa}^{-2}$
$\eta$	=	fatigue sensitivity index	-
$\sigma_m$	=	Mean Fatigue stress	$\text{MPa}$
$\sigma_a$	=	Fatigue stress amplitude	$\text{MPa}$
$\sigma_{ut}$	=	Ultimate tensile strength	$\text{MPa}$
$S_m$	=	The new modified stress level	-
$N$	=	The number of fatigue life cycles to failure	cycle